


Cite this: *RSC Adv.*, 2017, 7, 39635

# Synthesis, characterization and mechanism of formation of carbon aerogels incorporated with highly crystalline lanthanum oxychloride particles

Xiurong Zhu,<sup>a</sup> <sup>ab</sup> Yi Yu,<sup>a</sup> Jyjun Yuan,<sup>a</sup> Xianke Zhang,<sup>a</sup> Huajun Yu,<sup>a</sup> Wen Zhang,<sup>a</sup> Ai Du<sup>b</sup> and Bin Zhou<sup>b</sup>

Low-density monolithic carbon aerogels incorporated with highly crystalline lanthanum oxychloride (LaOCl) particles were successfully synthesized using a novel facile sol–gel method. The LaOCl-doped carbon aerogels were experimentally determined to be inorganic porous materials with a density of  $\sim 260 \text{ mg cm}^{-3}$ , specific surface area of  $465 \text{ m}^2 \text{ g}^{-1}$ , and average pore diameter of 28 nm. The embedded LaOCl particles were highly crystalline, having formed a tetragonal phase structure, and constituted up to 28.58% of the mass of the carbon aerogel. A sol–gel mechanism was proposed for the formation of the aerogel and included the acidity of an aqueous lanthanum chloride solution and ring opening of propylene oxide as two key factors promoting the formation of wet La-doped resorcinol-formaldehyde gels and highly crystalline LaOCl particles.

Received 14th May 2017

Accepted 6th July 2017

DOI: 10.1039/c7ra05454h

rsc.li/rsc-advances

## 1. Introduction

Lanthanum oxychloride (LaOCl) displays a matlockite tetragonal structure with the space group  $P4/nmm$  ( $Z = 2$ ). In this structure, the  $\text{La}^{3+}$  ion bonds four oxygen and five chlorine atoms.<sup>1</sup> Also, the  $\text{La}^{3+}$  ion has the largest ionic radius among the lanthanide (Ln) series of ions and can be easily substituted by other lanthanide ions as luminescent activators.<sup>2</sup> Therefore, LaOCl is an excellent host for various  $\text{Ln}^{3+}$  ( $\text{Ln} = \text{Nd}^{3+}$ ,  $\text{Tb}^{3+}$ ,  $\text{Eu}^{3+}$ ,  $\text{Yb}^{3+}$ ,  $\text{Sm}^{3+}$  and  $\text{Pr}^{3+}$ ) ions and has attracted considerable interest in applications such as phosphors, lamps, catalyst supports and gas sensors.<sup>3–6</sup> In addition, carbon aerogels and doped carbon aerogels display high surface areas, high porosity, fine pore size, and outstanding electrical conductivity, and hence have potential applications in areas like hydrogen storage, catalyst supports, electrodes, adsorption and supercapacitors.<sup>7–12</sup>

In recent years, many researchers have paid much attention to Ln-doped carbon aerogels because the addition of Ln species can enhance the structure, conductivity and catalytic activity of the aerogels. A series of Ln-doped carbon aerogels have been prepared by impregnation, ion exchange, precipitation, and sol–gel methods.<sup>13–16</sup>  $\text{CeO}_2$ -doped carbon aerogels have been prepared by applying a conventional sol–gel strategy and have been used as host materials for sulfur cathodes of lithium-sulfur batteries, the carbon aerogels

decorated with  $\text{CeO}_2$  not only suppress the loss of polysulfide ions, but display excellent rate performance.<sup>17</sup> La-, Ce-, Pr- and Nd-doped organic and carbon aerogels have been synthesized using the ion-exchange method, the amorphous doped organic and carbon aerogels have been tested as catalysts for the Michael reaction, and the 24 hour conversion rates of Ln-doped organic aerogels and Ln-doped carbon aerogels have been shown to be between 82 and 97% and between 32% and 92%, respectively.<sup>18</sup> Nevertheless, the synthesis, characterization, and sol–gel mechanism of formation of carbon aerogels incorporated with highly crystalline LaOCl particles have not been reported. Considering the excellent properties of LaOCl particles and carbon aerogels, LaOCl-doped carbon aerogels may be particularly good catalysts for the Michael reaction, hosts for  $\text{Ln}^{3+}$  ( $\text{Ln} = \text{Nd}^{3+}$ ,  $\text{Tb}^{3+}$ ,  $\text{Eu}^{3+}$ ,  $\text{Yb}^{3+}$ ,  $\text{Sm}^{3+}$  and  $\text{Pr}^{3+}$ ) ions, electrodes for lithium-based batteries, absorbents for automobile exhaust, and sensors for  $\text{CO}_2$  detection.

Herein, we present an attempt to prepare low-density LaOCl-doped carbon aerogels, in which the LaOCl particles are highly crystalline. Such a preparation has not been attempted previously to the best of our knowledge. By using propylene oxide (PO) as a catalyst, La-doped organic RF aerogels were first synthesized *via* a sol–gel process. LaOCl-doped carbon aerogels were then obtained by decomposing the La-doped RF aerogels. The density, composition, microstructure, specific surface area and pore size distribution of the La-doped RF aerogels and LaOCl-doped carbon aerogels were characterized, while the synthesis mechanisms of the LaOCl-doped carbon aerogels were demonstrated in detail.

<sup>a</sup>School of Physics and Electronic Information, Gannan Normal University, Ganzhou 341000, China. E-mail: zxr20786@hotmail.com

<sup>b</sup>Shanghai Key Laboratory of Special Artificial Microstructure Materials and Technology, Tongji University, Shanghai 200092, China



## 2. Experimental

### 2.1 Preparation of LaOCl-doped carbon aerogels

Fig. 1 shows the synthesis of LaOCl-doped carbon aerogels. First, a mass of 4.97 g resorcinol (R) was dissolved in 8.34 ml formaldehyde (F) to obtain a transparent RF solution. Then, a mass of 2.34 g of  $\text{LaCl}_3 \cdot 7\text{H}_2\text{O}$  was added into 20 ml deionized water to obtain a colorless  $\text{LaCl}_3$  solution. Finally, the  $\text{LaCl}_3$  solution was added dropwise into the RF solution. After 60 min, a volume of 5 ml propylene oxide (PO) was added into the mixture. Wet La-doped RF gels were obtained within 10 min, and then immersed in absolute ethanol for a week for solvent exchange. The resulting wet gels were removed from the ethanol solution and placed in an autoclave to carry out a  $\text{CO}_2$  supercritical drying process, during which monolithic La-doped RF aerogels formed. Under the protection of  $\text{N}_2$  atmosphere, monolithic LaOCl-doped carbon aerogels were acquired after the carbonization of the La-doped RF aerogels. The temperature and duration of the carbonization were  $1050^\circ\text{C}$  and 4 h, respectively.

### 2.2 Characterization of LaOCl-doped carbon aerogels

Scanning electron microscopy (SEM, Philips-XL30FEG) and transmission electron microscopy (TEM, Jeol JEM-2011) were used to characterize the microstructures of the La-doped RF aerogels and LaOCl-doped carbon aerogels. The compositions of these aerogels were determined by performing X-ray diffraction (XRD, Rigaku D/max2550VB3+/PC), energy dispersive X-ray spectroscopy (EDX, Jeol JEM-2011) and Fourier transform infrared spectrometry (FTIR, Bruker-TEN-SoR27). Their

isotherm adsorption/desorption curves, specific surface areas and pore distributions were acquired using a surface area and pore size analyzer (Quantachrome Autosorb-1-MP).

## 3. Results and discussion

### 3.1 Density and composition of the La-doped RF aerogels and LaOCl-doped carbon aerogels

Carbonization of the La-doped RF aerogels transformed them to LaOCl-doped carbon aerogels. Fig. 2(a) and (b) show photographs of the La-doped RF aerogels and LaOCl-doped carbon aerogels. Each of them maintained a good shape during the carbonization process. The diameters of the La-doped RF aerogels and LaOCl-doped carbon aerogels were measured to be about 1.7 cm and 1.3 cm, respectively, indicative of an  $\sim 24\%$  shrinkage resulting from the carbonization. The bulk densities of the La-doped RF aerogels and LaOCl-doped carbon aerogels were calculated after measuring their geometrical dimensions and weighing their masses at ambient laboratory conditions, and determined to be approximately  $192$  and  $260 \text{ mg cm}^{-3}$ , respectively. The increase ( $\sim 35\%$ ) in the density was attributed to the decomposition of organic material and shrinkage of volume during the pyrolysis.

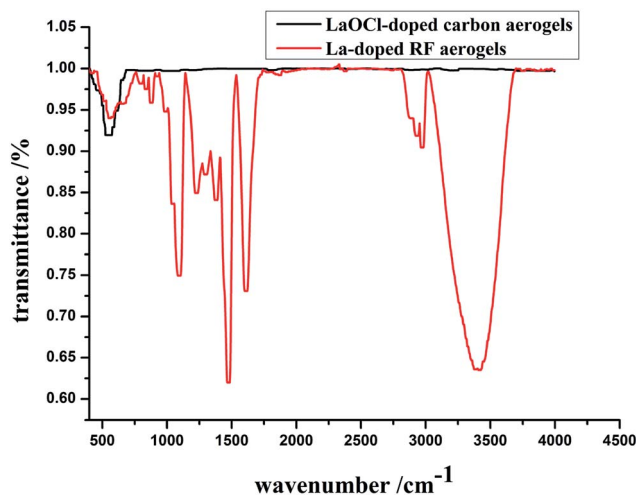


Fig. 3 FTIR traces of the La-doped RF aerogels (red) and LaOCl-doped carbon aerogels (black).

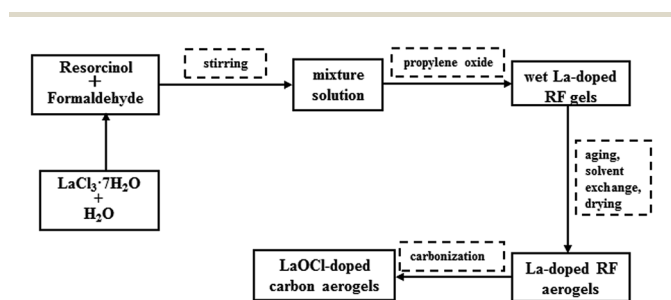


Fig. 1 Synthetic scheme for the La-doped RF aerogels and LaOCl-doped carbon aerogels.

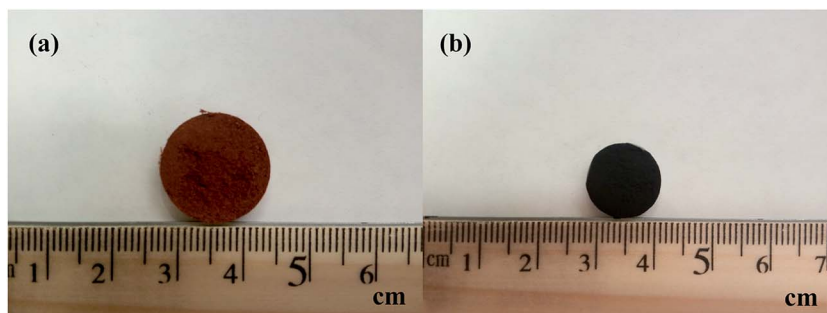


Fig. 2 Photographs of the La-doped RF aerogels (a) and LaOCl-doped carbon aerogels (b).



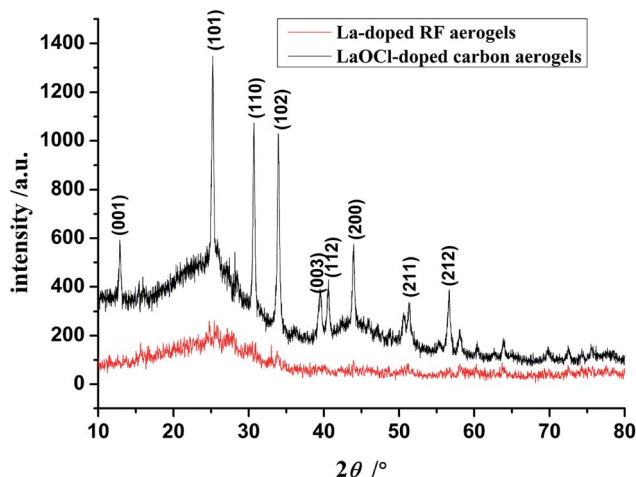


Fig. 4 XRD diffraction patterns of the La-doped RF aerogels (red) and LaOCl-doped carbon aerogels (black).

FTIR transmittance spectra of La-doped RF aerogels (red) and LaOCl-doped carbon aerogels (black) were acquired at room temperature from a wavenumber of 400 to that of 4000  $\text{cm}^{-1}$  and are shown in Fig. 3. In the two spectra, the fingerprint peak of the La–O bond was observed at about 540  $\text{cm}^{-1}$ , and was attributed to the stretching vibration.<sup>19</sup> The La-doped RF aerogels (red curve) also yielded other absorption peaks: those at 1100  $\text{cm}^{-1}$  and 1240  $\text{cm}^{-1}$  were attributed to C–O bonds from methylene ether bridges and from phenolic compounds, respectively,<sup>18</sup> those at 1330 and 2918  $\text{cm}^{-1}$  to C–H bending and stretching vibrations,<sup>20</sup> those at 1418 and 1600  $\text{cm}^{-1}$  detected due to  $\text{COO}^-$  carboxylate ion asymmetry stretching and symmetry vibration,<sup>21</sup> and that at 3420  $\text{cm}^{-1}$  due to the O–H bond from adsorbed water.<sup>22</sup>

To further confirm the nature of the lanthanum present in the carbon aerogels, XRD measurements were taken. Fig. 4 shows the XRD diffraction patterns of the La-doped RF aerogels

(red) and LaOCl-doped carbon aerogels (black). These data indicated the La-doped RF aerogels to be amorphous organic materials displaying low crystallinity. On the other hand, the LaOCl-doped carbon aerogels were highly crystalline. Although a broad diffraction peak due to amorphous carbon was observed in the XRD pattern of the LaOCl-doped carbon aerogels, major diffraction peaks were observed at  $2\theta = 12.8^\circ$ ,  $25.1^\circ$ ,  $30.7^\circ$ ,  $33.9^\circ$ ,  $39.2^\circ$ ,  $40.5^\circ$ ,  $43.9^\circ$ ,  $51.3^\circ$  and  $56.6^\circ$ , and corresponded to the reflection planes of (001), (101), (110), (102), (003), (112), (200), (211) and (212) respectively, which are consistent with the tetragonal phase structure with the space group  $P4/nmm$  ( $Z = 2$ ) (JCPDS file number: 08-0477). Neither any obvious shifting of peaks nor other impurity phase was observed in the X-ray data for the final product, and these results combined with the FTIR transmittance results indicated that the La-doped RF aerogels were completely converted to LaOCl-doped carbon aerogels after the 1050  $^\circ\text{C}$  pyrolysis under the protection of  $\text{N}_2$ .

Fig. 5 displays the EDX spectra of the LaOCl-doped carbon aerogels. Analysis of these EDX spectra showed that C, O, Cl and La were the main elements in the aerogels, and no other elements were found in the samples, indicating that the LaOCl-doped carbon aerogels were highly pure. Moreover, the mass percentages of C, O, Cl and La were calculated to be 71.42%, 2.14%, 6.02% and 20.42%, respectively, which indicated that the mass percentages of LaOCl and carbon particles were 28.58% and 71.42%.

### 3.2 Microstructures of the La-doped RF aerogels and LaOCl-doped carbon aerogels

Fig. 6(a) and (b) display the SEM micrographs of La-doped RF aerogels and LaOCl-doped carbon aerogels, respectively. Both aerogels were observed to have a three-dimensional network consisting of interconnected bead-like particles with diameters of several tens of nanometers. Both aerogels also showed good porosity, containing micropores, mesopores and macropores.

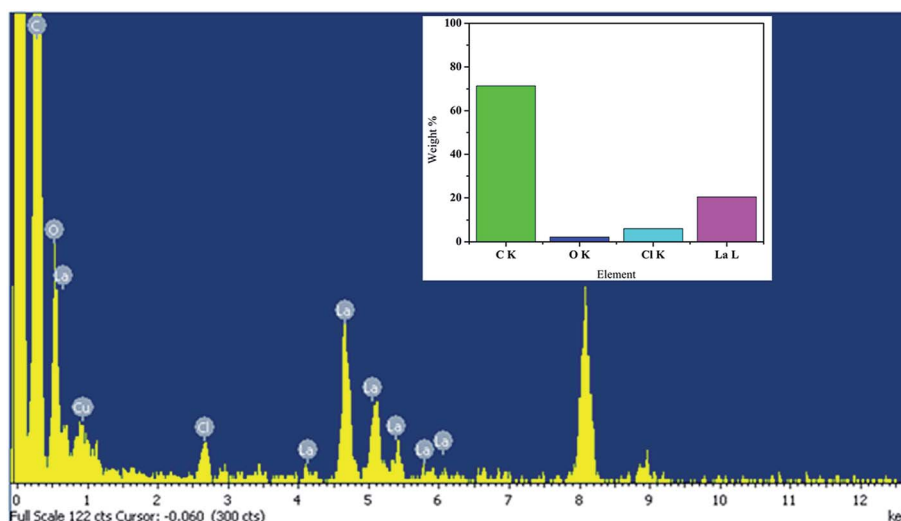


Fig. 5 EDX of the LaOCl-doped carbon aerogels.



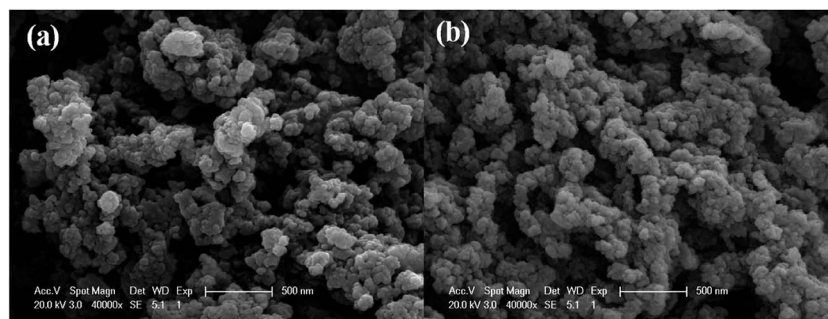


Fig. 6 SEM micrographs of the La-doped RF aerogels (a) and LaOCl-doped carbon aerogels (b).

The diameters of the pores of LaOCl-doped carbon aerogels were observed to be smaller than those of the La-doped RF aerogels, indicating that the particles of the aerogels became closer to each other as a result of the carbonization. A TEM image of the LaOCl-doped carbon aerogels is shown in Fig. 7(a). The dark particles were measured to have an average diameter of  $\sim 15$  nm and were identified as the LaOCl particles. The TEM image revealed that the LaOCl particles were homogeneously embedded in the networks of carbon aerogels. Fig. 7(b) shows the selected area electron diffraction (SAED) pattern of the LaOCl-doped carbon aerogels. The diffuse diffraction rings indicated the presence of amorphous carbon while the diffraction spots confirmed the formation of crystalline LaOCl particles. These results were consistent with the above analysis of the XRD patterns.

### 3.3 Specific surface area and pore size distributions of the La-doped RF aerogels and LaOCl-doped carbon aerogels

The  $N_2$  adsorption/desorption isotherms of the La-doped RF aerogels and LaOCl-doped carbon aerogels are shown in Fig. 8(a). Their isotherms were found to be close to type IV with their hysteresis loops consistent with the IUPAC type H3, de Boer type D,<sup>23,24</sup> which indicated the La-doped RF aerogels and LaOCl-doped carbon aerogels to have mesopores, while the adsorption  $P/P_0 = 0.1$  revealed the presence of micropores. The specific surface areas of the La-doped RF aerogels and LaOCl-

doped carbon aerogels were determined from BET evaluations to be about 573 and 465  $m^2 g^{-1}$ , *i.e.*, the specific surface area of the aerogels decreased by about 18.8% as a result of their being carbonized. Fig. 8(b) shows the pore size distribution curves derived from the desorption branches of the isotherms using the BJH method. The results revealed that both the La-doped RF aerogels and LaOCl-doped carbon aerogels contained many micropores, mesopores and macropores, and the peak values of the pore size of La-doped RF aerogels and LaOCl-doped carbon aerogels were about 48 and 40 nm, while their average pore diameters were 32 and 28 nm, respectively.

### 3.4 Sol-gel mechanism study of the La-doped RF aerogels and LaOCl-doped carbon aerogels

Reducing the gelation time of RF system to synthesize carbon aerogels is an important goal for basic research and commercial applications of carbon aerogels as well as metal-doped carbon aerogel. We have always observed the formation of wet RF gels to take several days for the reaction catalyzed by base, but only a few hours when catalyzed by acid.<sup>14</sup> During the preparation of La-doped RF aerogels, the  $LaCl_3$  aqueous solution became acidic, which may have been due to the reactions shown in eqn (1) and (2) having reached equilibrium. It was the acidity that forced the R and F preparing system to gel within 10 min. PO ( $C_3H_6O$ ) is well known as a proton ( $H^+$  ion) scavenger and gelling agent to prepare metal oxide aerogels without using

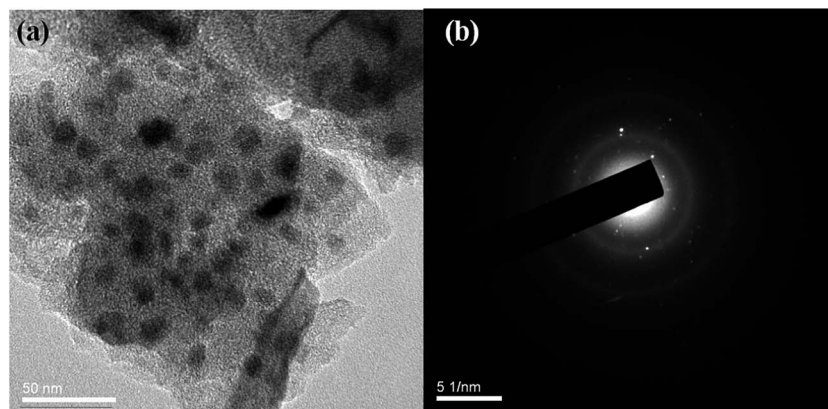


Fig. 7 (a) TEM and (b) SAED pattern of the LaOCl-doped carbon aerogels.





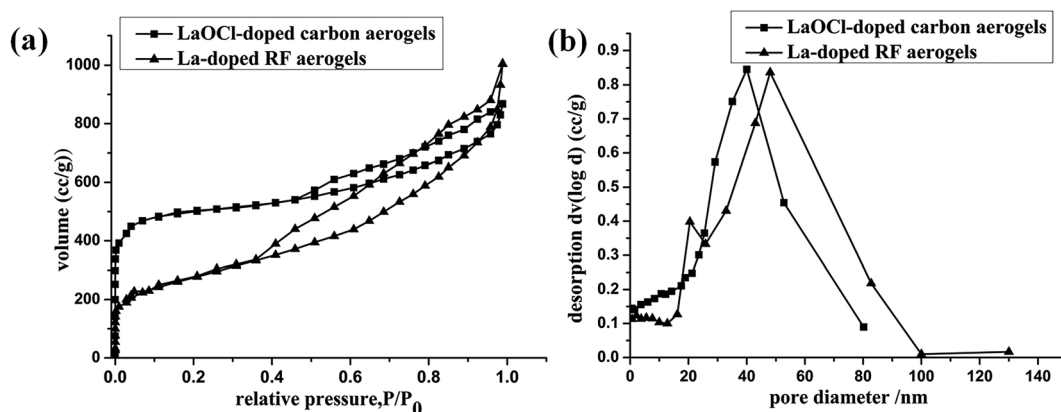
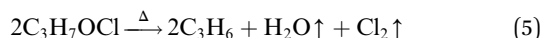
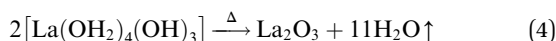
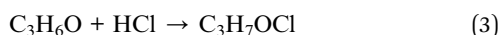
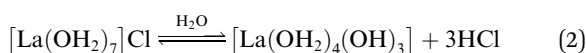
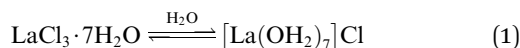


Fig. 8 (a)  $N_2$  adsorption/desorption isotherms and (b) pore size distribution curves.

alkoxide.<sup>25</sup> When PO was added to a mixture of R, F,  $LaCl_3$  and  $H_2O$ , the HCl in the solution was rapidly consumed by the ring-opening reaction of PO (see eqn (3)). At the same time, the pH of the mixture increased, which promoted the formation of the  $La(OH_2)_4(OH)_3$  product of reaction shown in eqn (2) and of wet La-doped RF gels.<sup>26</sup> Along with the transformation of RF to C in the carbonization of the La-doped RF aerogels, the  $La(OH_2)_4(OH)_3$  was converted to  $La_2O_3$  (see eqn (4)) and  $Cl_2$  was simultaneously produced from the decomposition of the reaction byproduct  $C_3H_7OCl$  (see eqn (5)). Finally, the LaOCl was obtained in the presence of  $La_2O_3$  and  $Cl_2$  (see eqn (6)).<sup>27</sup>



## 4. Conclusions

By using R, F,  $LaCl_3$ ,  $H_2O$  and PO as precursors, LaOCl-doped carbon aerogels were synthesized *via* a sol-gel process, which may provide a general method for rapidly preparing metal-doped carbon aerogels. LaOCl particles with high crystallinity were homogeneously embedded into the networks of carbon aerogels. Up to 28.58% of the mass of the LaOCl-doped carbon aerogel was found to be LaOCl particles, and the percentage may be increased further by adjusting the relative amounts of the different precursors. Carbonization of the amorphous La-doped RF aerogel led to its complete transformation to the LaOCl-doped carbon aerogel, and this process was accompanied by an  $\sim 24\%$  decrease in the volume,  $\sim 35\%$  increase in

density, and  $\sim 19\%$  decrease in the specific surface area of the aerogel. The acidity of the  $LaCl_3$  aqueous solution and the ring-opening of PO played important roles in the formation of wet La-doped RF gels and highly crystalline LaOCl particles.

## Acknowledgements

This research was financially supported by the National Natural Science Foundation of China (No. 51302040, 11647101) and the Youth Fund of Science and Technology Department of Jiangxi Province (No. GJJ13652, GJJ160940). The authors are very grateful for this support.

## References

- 1 J. Holsa and P. Porcher, *J. Chem. Phys.*, 1981, **75**, 2108–2117.
- 2 J. Holsa, M. Lahtinen, M. Lastusaari, J. Valkonen and J. Viljanen, *J. Solid State Chem.*, 2002, **165**, 48–55.
- 3 Y. D. Eagleman, E. Bourret-Courchesne and S. E. Derenzo, *J. Lumin.*, 2011, **131**, 669–675.
- 4 J. S. Im, M. Il Kim and Y. S. Lee, *Mater. Lett.*, 2008, **62**, 3652–3655.
- 5 A. Marsal, E. Rossinyol, F. Bimbela, C. Tellez, J. Coronas, A. Cornet and J. R. Morante, *Sens. Actuators, B*, 2005, **109**, 38–43.
- 6 U. Rambabu, T. Balaji, K. Annapurna and S. Buddhudu, *Mater. Chem. Phys.*, 1996, **43**, 195–198.
- 7 M. Antonietti, N. Fechner and T. P. Fellingner, *Chem. Mater.*, 2014, **26**, 196–210.
- 8 Y. J. Hu, X. Tong, H. Zhuo, L. X. Zhong, X. W. Peng, S. Wang and R. C. Sun, *RSC Adv.*, 2016, **6**, 15788–15795.
- 9 C. Moreno-Castilla and F. J. Maldonado-Hodar, *Carbon*, 2005, **43**, 455–465.
- 10 R. W. Pekala, J. C. Farmer, C. T. Alviso, T. D. Tran, S. T. Mayer, J. M. Miller and B. Dunn, *J. Non-Cryst. Solids*, 1998, **225**, 74–80.
- 11 R. Saliger, U. Fischer, C. Herta and J. Fricke, *J. Non-Cryst. Solids*, 1998, **225**, 81–85.
- 12 G. Q. Zu, J. Shen, Z. H. Zhang, B. Zhou, X. D. Wang, G. M. Wu and Y. W. Zhang, *RSC Adv.*, 2017, **7**, 10583–10591.



- 13 E. Bekyarova and K. Kaneko, *Langmuir*, 1999, **15**, 7119–7121.
- 14 E. Bekyarova and K. Kaneko, *Adv. Mater.*, 2000, **12**, 1625–1628.
- 15 S. Martinez, L. Martin, E. Molins, M. Moreno-Manas, A. Roig and A. Vallribera, *Monatsh. Chem.*, 2006, **137**, 627–633.
- 16 N. Leventis, N. Chandrasekaran, A. G. Sadekar, S. Mulik and C. Sotiriou-Leventis, *J. Mater. Chem.*, 2010, **20**, 7456–7471.
- 17 X. L. Li, L. S. Pan, Y. Y. Wang and C. S. Xu, *Electrochim. Acta*, 2016, **190**, 548–555.
- 18 K. Kreek, K. Kriis, B. Maaten, M. Uibu, A. Mere, T. Kanger and M. Koel, *J. Non-Cryst. Solids*, 2014, **404**, 43–48.
- 19 A. K. Zak, W. H. Abd Majid and M. Darroudi, *Mater. Chem. Phys.*, 2012, **136**, 705–709.
- 20 M. Xu, Y. Y. Ao, S. J. Wang, J. Peng, J. Q. Li and M. L. Zhai, *Carbohydr. Polym.*, 2015, **128**, 171–178.
- 21 S. Sitthichai, C. Pilapong, T. Thongtem and S. Thongtem, *Appl. Surf. Sci.*, 2015, **356**, 972–977.
- 22 L. M. S. El-Deen, M. S. Al Salhi and M. M. Elkholy, *J. Alloys Compd.*, 2008, **465**, 333–339.
- 23 J. C. Broekhoff and J. H. Deboer, *J. Catal.*, 1968, **10**, 391–400.
- 24 K. S. W. Sing, *Pure Appl. Chem.*, 1982, **54**, 2201–2218.
- 25 P. D. Brown, S. K. Gill and L. J. Hope-Weeks, *J. Mater. Chem.*, 2011, **21**, 4204–4208.
- 26 A. E. Gash, J. H. Satcher and R. L. Simpson, *J. Non-Cryst. Solids*, 2004, **350**, 145–151.
- 27 J. P. Gaviria, L. G. Navarro and A. E. Bohe, *J. Phys. Chem. A*, 2012, **116**, 2062–2070.

